The Journal of Immunology

HLA-DRα1 Constructs Block CD74 Expression and MIF Effects in Experimental Autoimmune Encephalomyelitis

Roberto Meza-Romero, Gil Benedek, Xiaolin Yu, Jeffery L. Mooney, Rony Dahan, Nerri Duvshani, Richard Bucala, Halina Offner, Yoram Reiter, Gregory G. Burrows and Arthur A. Vandenbark

J Immunol 2014; 192:4164-4173; Prepublished online 28 March 2014;
doi: 10.4049/jimmunol.1303118
http://www.jimmunol.org/content/192/9/4164

The Journal of Immunology is published twice each month by
The American Association of Immunologists, Inc.,
1451 Rockville Pike, Suite 650, Rockville, MD 20852

Print ISSN: 0022-1767 Online ISSN: 1550-6606.

HLA-DRα1 Constructs Block CD74 Expression and MIF Effects in Experimental Autoimmune Encephalomyelitis

Roberto Meza-Romero,[*,†,1] Gil Benedek,[*,†,1] Xiaolin Yu,[*,†] Jeffery L. Mooney,[‡] Rony Dahan,[§] Nerri Duvshani,[§] Richard Bucala,[¶] Halina Offner,[*,†,‖] Yoram Reiter,[§] Gregory G. Burrows,[#,] and Arthur A. Vandenbark[*,†,††,‡‡]**

CD74, the cell-surface form of the MHC class II invariant chain, is a key inflammatory factor that is involved in various immune-mediated diseases as part of the macrophage migration inhibitory factor (MIF) binding complex. However, little is known about the natural regulators of CD74 in this context. In order to study the role of the HLA-DR molecule in regulating CD74, we used the HLA-DRα1 domain, which was shown to bind to and downregulate CD74 on CD11b$^+$ monocytes. We found that DRα1 directly inhibited binding of MIF to CD74 and blocked its downstream inflammatory effects in the spinal cord of mice with experimental autoimmune encephalomyelitis (EAE). Potency of the DRα1 domain could be destroyed by trypsin digestion but enhanced by addition of a peptide extension (myelin oligodendrocyte glycoprotein [MOG]-35–55 peptide) that provided secondary structure not present in DRα1. These data suggest a conformationally sensitive determinant on DRα1-MOG that is responsible for optimal binding to CD74 and antagonism of MIF effects, resulting in reduced axonal damage and reversal of ongoing clinical and histological signs of EAE. These results demonstrate natural antagonist activity of DRα1 for MIF that was strongly potentiated by the MOG peptide extension, resulting in a novel therapeutic, DRα1–MOG-35–55, that within the limitations of the EAE model may have the potential to treat autoimmune diseases such as multiple sclerosis. ***The Journal of Immunology*****, 2014, 192: 4164–4173.**

The class II invariant chain (Ii; CD74) not only chaperones peptide-loaded MHC class II molecules from intracellular compartments to the surface of APCs but also functions as the receptor for macrophage migration inhibitory factor (MIF) when expressed on the cell surface (1, 2). MIF engagement of CD74 leads to the recruitment and activation of CD44 and CXCR2/4 to initiate signaling pathways necessary for MAPK activation and cell motility (3–5). We recently demonstrated enhanced CD74 cell-surface expression on monocytes in mice with experimental autoimmune encephalomyelitis (EAE) and subjects with multiple sclerosis (MS), which implicates its involvement in the disease course (6).

Although it has been shown that MIF binds to the CD74 extracellular domain, the actual binding site is not known. In addition, little has been reported on natural anti-inflammatory regulators that can inhibit MIF/CD74 signaling either by downregulating CD74 cell-surface expression or blocking MIF binding (7, 8). Moreover, it is not clear if interactions between MHC class II and CD74 on the cell surface influence MIF binding and subsequent signal transduction events.

We previously reported that the DRα1 domain but not the DR2β1 domain binds immunoprecipitated CD74. In the current study, we used the DRα1 domain to study the interaction of this domain with CD74, its effect on MIF binding and signaling, and its potential use as a novel therapeutic reagent.

We report in this study that the HLA class II DRα1 domain binds to human and mouse monocytes through cell-surface CD74 and that this interaction inhibits MIF binding and signaling. This interaction may be potentially exploited as a treatment for MIF-dependent CNS diseases. Potency of the DRα1 domain was eliminated by trypsin digestion but enhanced by addition of a peptide extension (myelin oligodendrocyte glycoprotein [MOG]-35–55 peptide) at the N terminus that provided discrete secondary α-helical and β-sheet structure. These data suggest a conformationally sensitive determinant on DRα1 for which the structure is influenced by an N-terminal MOG peptide extension. We hypothesize that this conformation is responsible for optimal binding of DRα1 to CD74 and antagonism of MIF action, which resulted in reversal of clinical and histological signs of EAE. Moreover,

*Neuroimmunology Research, Department of Veterans Affairs Medical Center, Portland, OR 97239; †Tykeson Multiple Sclerosis Research Laboratory, Department of Neurology, Oregon Health & Science University, Portland, OR 97239; ‡Department of Pediatrics, Oregon Health & Science University, Portland, OR 97239; §Faculty of Biology, Technion-Israel Institute of Technology, Haifa 3200003, Israel; ¶Section of Rheumatology, Department of Internal Medicine, Yale University School of Medicine, New Haven, CT 06520; ‖Department of Anesthesiology and Perioperative Medicine, Oregon Health & Science University, Portland, OR 97239; #Department of Biochemistry, Oregon Health & Science University, Portland, OR 97239; **Hematology and Medical Oncology Services, Knight Cancer Institute, Oregon Health & Science University, Portland, OR 97239; ††Department of Molecular Microbiology & Immunology, Oregon Health & Science University, Portland, OR 97239; and ‡‡Research Service, Department of Veterans Affairs Medical Center, Portland, OR 97239

[1]R.M.-R. and G.B. contributed equally to this manuscript.

Received for publication November 19, 2013. Accepted for publication February 25, 2014.

This work was supported by National Institutes of Health Grants NS47661 (to A.A.V.) and AR050498 (to R.B.), National Multiple Sclerosis Society Grant RG3794-B-6 (to A.A.V.), a postdoctoral fellowship from the National Multiple Sclerosis Society (to G.B.), an Oregon Medical Research Foundation grant (to G.B.), and the Department of Veterans Affairs, Veterans Health Administration, Office of Research and Development, Biomedical Laboratory Research and Development.

The contents do not represent the views of the Department of Veterans Affairs or the U.S. Government.

Address correspondence and reprint requests to Dr. Arthur A. Vandenbark, Research Service R&D31, Department of Veterans Affairs Medical Center, 3710 SW US Veterans Hospital Road, Portland, OR 97239. E-mail address: vandenba@ohsu.edu

The online version of this article contains supplemental material.

Abbreviations used in this article: A488, Alexa 488; CD, circular dichroism; CDI, Cumulative Disease Index; EAE, experimental autoimmune encephalomyelitis; HC, healthy control; H2-M, mouse homolog of human HLA-DM; Ii, class II invariant chain; MIF, macrophage migration inhibitory factor; MS, multiple sclerosis; Ptx, pertussis toxin; PVDF, polyvinylidene difluoride; rh, recombinant human; TEN, 50 mM Tris, 2 mM EDTA, and 150 mM NaCl; Tg, transgenic; TSST-1, toxic shock syndrome toxin 1.

www.jimmunol.org/cgi/doi/10.4049/jimmunol.1303118

because the invariable DRα1 domain is present in all human subjects and would not be recognized as immunologically foreign, treatment with DRα1 constructs would not require HLA screening prior to injection and could be universally applicable as therapy for CNS or other inflammatory diseases.

Materials and Methods

Human PBMC

Peripheral blood was obtained from healthy control (HC) donors who were screened for HLA genotype. The study protocol received institutional review board approval. All participants signed an informed consent. PBMCs were obtained by centrifugation through Ficoll (Histopaque 1077; Sigma-Aldrich). Samples were stored in liquid nitrogen until used.

Mice

DR*1501-transgenic (Tg) and MBP-TCR/DR2-Tg mice were bred in-house at the Veterinary Medical Unit, Portland Veterans Affairs Medical Center, and used at 8–12 wk of age. All procedures were approved and performed according to institutional guidelines.

DRα1 and DRα1-MOG cloning, production, and purification

The DRα1 domain cloning, production, and purification has been described previously (9). DRα1-MOG was built using the α1 domain construct as a template. The human MOG-35–55 peptide DNA-encoding sequence was attached to the N terminus of the DRα1 domain with a linker–thrombin cleavage site–linker intervening element. The single-chain gene was cloned into the NcoI and XhoI restriction sites of the pET21d(+) vector (Novagen) and transformed into *Escherichia coli* BL21 (DE3) expression host (New England Biolabs). For protein production, 4 L Luria-Bertani medium, supplemented with 50 μg/ml carbenicillin, was inoculated with a starting OD_{600} of 0.05. Isopropyl β-D-thiogalactoside was added when the culture reached 0.7 OD_{600}. Cultures were allowed to grow for 4 h and then ice-chilled before harvesting at 7000 rpm for 6 min. After centrifugation, the pellet was resuspended in lysis buffer (50 mM Tris, 5 mM EDTA, and 300 mM NaCl [pH 8]), treated with lysozyme (1 ml at 10 mg/ml) for 30 min at room temperature, and lysed in ice by sonication in a Branson Sonifier 450 apparatus with pulses of 1 min and pauses of 5 min. The disrupted suspension was pelleted at 7000 rpm for 6 min, and the paste was resuspended in 1% Triton X-100 in lysis buffer to remove lipids and other hydrophobic contaminants. Detergent was removed by resuspending the pellet lysis buffer followed by sonication as described earlier. This was repeated three more times. The final pellet was solubilized in Buffer A (20 mM ethanolamine and 6 M Urea [pH 10]) overnight at 4°°C and then spun down at 40,000 × *g* to remove particulate material. This lysate was filtered through a 0.22-μm filter twice and loaded onto a Mono-Q anion-exchange 50-ml column at a flow rate of 2 ml/min attached to an AKTA FPLC (GE Healthcare). After washing the column until no eluting material was detected at 280 nm, proteins were eluted by applying a stepwise gradient of 2 M NaCl in buffer A. The eluate was collected in fractions of 8 ml, and after electrophoretic analysis, those containing the target protein were pooled together. This pooled material was concentrated with a 3-kDa MWCO membrane (Millipore), filtered twice through a 0.22-μm membrane, and then loaded onto a Superdex 75, 16/60 size-exclusion column (GE Healthcare). The loaded protein was eluted with buffer C (20 mM ethanolamine, 4 mM NaCl, and 6 M Urea [pH 10]) at a flow rate of 1 ml/min, collected into fractions of 1 ml, and finally dialyzed against 20 mM Tris (pH 8.5) for refolding. After refolding, the DRα1-MOG protein was concentrated to 10 mg/ml, snap-frozen, and stored in 1-ml aliquots at −80°C until use.

Binding of DRα1 to immunopurified CD74 and mouse equivalent of HLA-DM

CD74 and mouse homolog of human HLA-DM (H2-M) were serially captured from a CHAPS lysate of DR*1501-Tg mouse splenocytes using 2 μg rat anti-mouse CD74 (clone ln-1) and rat anti-mouse H2-M (clone 2E5A) mAbs (BD Pharmingen, San Diego, CA) adsorbed to Protein L Beads. DRα1 was labeled with fluorescent chromophore Alexa 488 (A488). A488-DRα1 (either undigested or digested with trypsin) binding to CD74 or H2-M–conjugated beads was evaluated by quantification of A488-DRα1 eluted from the binding reaction as analyzed by Tris-Tricine peptide gel electrophoresis and visualized by fluorescent scanning at 488 nm with a Molecular Imager X (Bio-Rad).

Microscopy imaging of DRα1 binding

Two million $CD11b^+$ cells were negatively isolated from DR*1501/GFP-Tg mice by the Mouse Monocyte Enrichment Kit (StemCell Technologies) and treated with 10 μg/ml DRα1 tagged with Alexa 546. The images were acquired on a high-resolution wide-field Core DV system (Applied Precision) using an Olympus IX71 inverted microscope with a proprietary XYZ stage enclosed in a controlled environment chamber (Olympus), transmitted-light differential interference contrast, and a solid-state module for fluorescence. A Nikon Coolsnap ES2 HQ (Nikon) was used to acquire images as optical axis with a 60× (numerical aperture 1.42) Plan-Apo N objective in two colors, FITC, and tetramethylrhodamine isothiocyanate. The pixel size was 0.10704 microns. The images were deconvolved with the appropriate optical transfer function using an iterative algorithm of 10 iterations. Histograms were optimized for the most positive image and applied to all the other images for consistency before saving the images as 24-bit merged TIF files.

Induction of EAE in DR2-Tg and MBP-TCR/DR2-Tg mice

Mice were screened by flow cytometry for the expression of the HLA and the TCR transgenes (10). HLA-DR2–positive male and female mice between 8 and 12 wk of age were immunized s.c. at four sites on the flanks with 0.2 ml emulsion of 200 μg immunogenic peptide and CFA containing 400 μg heat-killed *Mycobacterium tuberculosis* H37RA (Difco, Detroit, MI) (10). In addition, mice were given pertussis toxin (Ptx) from List Biological Laboratories (Campbell, CA) on days 0 and 2 post-immunization (75 and 200 ng/mouse, respectively). Immunized mice were assessed daily for clinical signs of EAE on a six-point scale of combined hind limb and forelimb paralysis scores. For hind limb scores: 0, normal; 0.5, limp tail or mild hind limb weakness (i.e., a mouse cannot resist inversion after a 90° turn of the base of the tail); 1, limp tail and mild hind limb weakness; 2, limp tail and moderate hind limb weakness (i.e., an inability of the mouse to rapidly right itself after inversion); 3, limp tail and moderately severe hind limb weakness (i.e., inability of the mouse to right itself after inversion and clear tilting of hind quarters to either side while walking); 4, limp tail and severe hind limb weakness (hind feet can move but drag more frequently than face forward); and 5, limp tail and paraplegia (no movement of hind limbs). Front limb paralysis scores are either 0.5 for clear restriction in normal movement or 1 for complete forelimb paralysis. The combined score is the sum of the hind limb score and the forelimb score. Rarely, there is mortality of HLA-DR2 mice with severe EAE, and in these cases, mice are scored as a 6 for the remainder of the experiment. Mean EAE scores and SDs for mice grouped according to initiation of RTL or vehicle treatment were calculated for each day and summed for the entire experiment (Cumulative Disease Index [CDI] represents total disease load). Daily mean scores were analyzed by a two-tailed Mann–Whitney *U* test for nonparametric comparisons between vehicle and RTL treatment groups. Mean CDIs were analyzed by a one-way ANOVA with Tukey posttest and a nonparametric one-way Kruskal-Wallis ANOVA with Dunn multiple comparisons posttest to confirm significance among all groups.

DRα1 or DRα1–MOG-35–55 treatment of EAE in DR2-Tg mice

DRα1 constructs were injected s.c. daily for 5 d at indicated doses to treat EAE induced in Tg mice, and clinical signs were scored as described above.

Flow cytometry

Four-color (FITC, PE, propidium iodide, allophycocyanin) fluorescence flow cytometry analyses were performed to determine the phenotypes of cells following standard Ab staining procedures. At indicated time points, cardiac blood was collected in EDTA followed by perfusion of the mice with 1× PBS. For splenocytes, single-cell suspensions of spleens from vehicle and DRα1 treatment groups were prepared by homogenizing the tissue through a fine mesh screen. Blood cells were pelleted after lysis of red cells, followed by washing twice with RPMI 1640. Mononuclear cells from the spinal cord were isolated by Percoll gradient centrifugation as described (11). Cells from spleen, blood, and spinal cord were resuspended in staining medium (5% BSA, 1× PBS, and 0.02% sodium azide) for FACS staining. All Abs were purchased from BD Pharmingen, eBioscience (San Diego, CA), or Santa Cruz Biotechnology (Santa Cruz, CA) unless otherwise indicated. Cells were stained with a combination of fluorescent-labeled Abs to CD11b, CD74, and CD45. For assessing DRα1 binding, 1 million cells were incubated in RPMI 1640 with 5 μg DRα1–A488 for 1 h at 37°C. All

incubations were followed directly by a 30-min incubation at 4˚C with anti-CD11b allophycocyanin (BD Pharmingen), After staining, cells were washed with staining medium and analyzed immediately with an FACS-Calibur (BD Biosciences) using FCS express software. Data represent 10,000 live-gated monocytes. Absolute numbers of cells were calculated from live-gated spinal cord cells.

Binding of recombinant human MIF to immunopurified CD74

Recombinant human (rh)MIF was prepared from an *E. coli* expression system and purified free of endotoxin by methods described previously (12). rhMIF was labeled with Alexa Fluor 488 (Invitrogen) following the manufacturer's instructions. CD74 complexes were immune-adsorbed from a CHAPS-solubilized lysate from splenocytes from DR*1501-Tg mice as described elsewhere. Briefly, after lysis, splenocytes were centrifuged at 14,000 rpm to remove debris, and the supernatant was mixed with Beads/Protein L-adsorbed anti-CD74 overnight at 4˚C. Immune complexes were washed extensively, and the CD74 complexes were left adsorbed to the beads. To assess the effect of the DRα1 on rhMIF/CD74 binding, 10 pmol rhMIF-A488 or 10 pmol rhMIF-A488 plus 0.3 or 1 nmol DRα1 or DR2β1 was bound to ln-1–immunoadsorbed CD74 for 16 h at 4˚C in 0.01% CHAPS/50 mM Tris, 2 mM EDTA, and 150 mM NaCl (TEN [pH 7.4]) buffer. Proteins were eluted by incubating the beads with 2% SDS-electrophoresis sample buffer at 98˚C for 7 to 8 min, and the material was separated by electrophoresis in a 10–20% SDS-PAGE. Before blotting to the polyvinylidene difluoride (PVDF) membrane, the gel was scanned for A488 to locate and quantify bound rhMIF. The PVDF membrane was blocked with 3% BSA/PBS containing 0.05% Tween 20 and probed with ln-1 mAb conjugated to FITC for 4 to 5 h at 4˚C. The membrane was scanned for FITC, and CD74 bands of expected m.w. were localized. DRα1 bands were localized in the membrane after Coomassie blue staining of the gels.

Electrophoresis and Western blot

Samples were analyzed by reducing and nonreducing Laemli SDS-PAGE and, when necessary, blotted onto PVDF at 400 mA for 45 min. Membranes then were blocked with 3% BSA in PBS and 0.05% Tween 20 either for 3 h or overnight before probing with the appropriate Ab.

Circular dichroism spectrometry

Before circular dichroism (CD) analysis, DRα1, DRα1–MOG-35–55, DR2β1, and the MOG-35–55 peptide were dialyzed in 20 mM Tris buffer (pH 8.5) and adjusted to a concentration of 1 mg/ml. Proteins were >95% pure as assessed by SDS-PAGE under nonreducing conditions. Far UV (180–260 nm) spectra of the samples were run on an AVIV Model 215 circular dichroism spectropolarimeter at 0.5- or 1-nm intervals using a 0.1-cm light path with a 3-s average time in triplicate at 25˚C. For deconvolution, the blank (20 mM Tris [pH 8.5]) average readings were subtracted from the sample average readings and plotted as molar ellipticity.

Histology

Mice were deeply anesthetized with isoflurane, heparinized and perfused with 100 ml 4% paraformaldehyde in 0.1 M sodium phosphate buffer (pH 7.4), and fixed at 4˚C for 24 h. The spinal cords were dissected from the spinal columns and sectioned 1 to 2 mm in length from cervical, thoracic, and lumbar cords. Tissues were placed in 0.1 M sodium phosphate buffer (pH 7.4), immersed and fixed with 5% glutaraldehyde in 0.1 M sodium phosphate buffer (pH 7.4) for 3 d at 4˚C, postfixed with 1% osmium tetroxide (in 0.1 M phosphate buffer) for 3.5 h, dehydrated in ethanol, and embedded in plastic. Semithin sections (0.5 μm) were stained with toluidine blue and photographed using a light microscope.

$CD4^+$ and $CD11b^+$ cell cocultures

Spleens were collected from MBP-TCR/DR2-Tg mice 9 d after immunization (as described before) (13) with MBP-85-99/CFA/Ptx. $CD4^+$ and $CD11b^+$ cells were negatively isolated (StemCell Technologies). Cell purity was >85%. CFSE-labeled MBP-85–99-specific $CD4^+$ T cells were cocultured with $CD11b^+$ cells at a 1:2 ratio (for $CD11b^+$) in 96-well round-bottom plates for 3 d at 37˚C in the presence of MBP-85–99 and/or DRα1 or DRα1–MOG-35–55. Following incubation, cells were harvested, washed, and stained with fluorescent-labeled anti-CD3 to study T cell proliferation concomitant with CFSE dilution.

Statistical analysis

Statistical analysis was performed using the Mann–Whitney *U* test and Student *t* test, unless mentioned otherwise. Values of $p < 0.05$ were considered significant.

Results

DRα1 binds to CD74 and H2-M

We recently have demonstrated that the DRα1 but not the DR2β1 domain binds to immunopurified CD74 (9). Experimental and crystallographic studies have shown that MHC class II interacts with Ii (CD74) and H2-M (HLA-DM in humans) in different subcellular compartments, and they have shown that the contact region is mainly located in the MHC α1 domain (14–16). Thus, the DRα1 domain was tested for binding activity to these membrane-anchored proteins using in vitro assays with immuno-

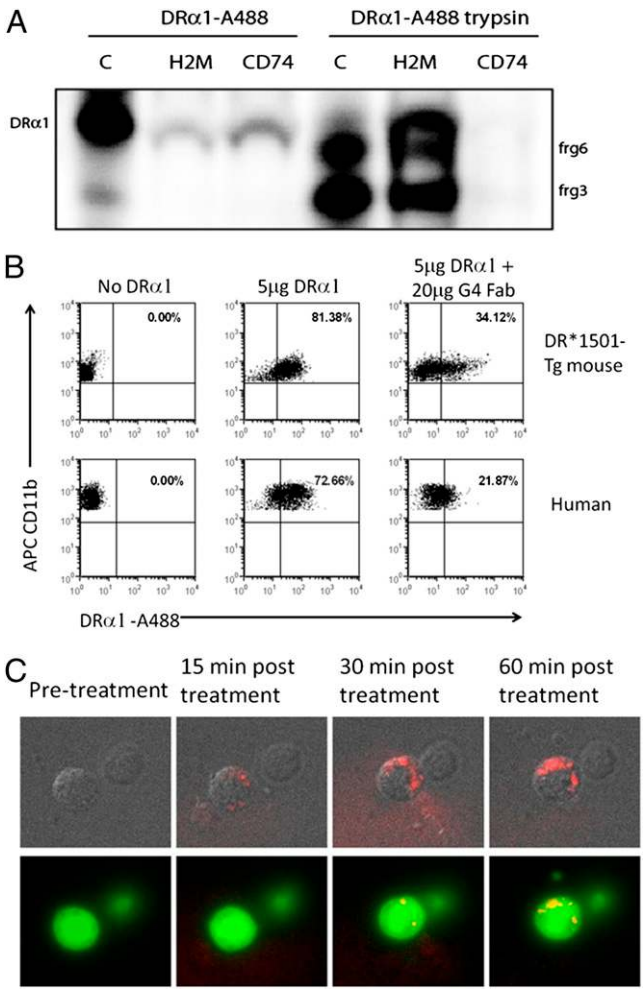

FIGURE 1. Binding of DRα1 to immunopurified CD74 and H2-M molecules and to $CD11b^+$ monocytes. (**A**) DRα1 domain binds to H2-M and CD74 but trypsin-digested DRα1 fragments bind solely to H2-M. DRα1 domain was labeled with A488 for 2 h at room temperature and digested with trypsin for 2 h at room temperature in 20 mM Tris (pH 8.5). Undigested or digested labeled DRα1 was then bound to immunoprecipitated H2-M and CD74 for 16–18 h at 4˚C in 1% CHAPS in TEN buffer, and the material bound to immunoprecipitated complexes was visualized by electrophoresis in a 10–20% Tris-Tricine PAGE with 2% SDS. Intact DRα1 binds with higher efficiency to CD74 compared with H2-M, but peptides generated by trypsin digestion of DRα1 bind exclusively to H2-M and not to CD74. *Lane C* contains labeled undigested and digested proteins that were run as a control. (**B**) Human PBMC from HC and blood cells from DR*1501-Tg mice were incubated with 5 μg DRα1–A488 for 1 h at 37˚C. To neutralize DRα1 binding, 5 μg DRα1–A488 was incubated at a 1:1 molar ratio (20 μg) of FabG4 for 2 h at room temperature prior to incubation with cells. $CD11b^+$ monocytes were then analyzed for DRα1 binding by FACS. (**C**) Isolated GFP^+CD11b^+ cells from DR*1501/GFP-Tg mice were treated with 10 μg DRα1–A546 for 60 min and evaluated by fluorescence microscopy.

precipitated CD74 and H2-M from DR*1501-Tg mouse splenocytes. As shown in Fig. 1A, the recombinant DRα1 domain bound to both CD74 and H2-M. Digestion of DRα1 with trypsin yielded fragments that could still bind to H2-M but not to CD74, suggesting different structural requirements for binding of the DRα1 fragments to each of these molecules. These data suggest that the DRα1 constructs mimic the binding properties of the full-length HLA-DR molecule and provide a binding interface for both CD74 and HLA-DM.

DRα1 construct binds mouse and human monocytes

To further study the interaction of DRα1 with cell-surface CD74 and determine if DRα1 could bind to mouse and human cells, blood cells from DR*1501-Tg mouse or PBMC from an HLA-DR2$^+$ HC donor were incubated for 1 h with DRα1-A488 with or without a Fab construct that is specific for binding the DRα1 construct (FabG4), as shown in Supplemental Fig. 1. Both mouse and human CD11b$^+$ monocytes bound the labeled DRα1 construct (81 and 73% positive, respectively), and this binding was strongly but not completely inhibited (reduced to 34 and 22% positive, respectively) when DRα1 was incubated with FabG4 at a 1:1 molar ratio for 2 h (Fig. 1B) prior to cell binding. In addition, as demonstrated in Supplemental Fig. 2, CD3$^+$ T cells from DR*1501-Tg mice expressed very low levels of cell-surface CD74 (~4.5%) and had low binding levels of DRα1-A488 (~6%) as compared with CD11b$^+$ cells (97% expression of CD74 and 80% binding of DRα1-A488), demonstrating an association between CD74 expression and degree of DRα1-A488 cell binding.

Direct binding of labeled DRα1 construct to GFP$^+$CD11b$^+$ monocytes, isolated from DR*1501/GFP-Tg mice and visualized by fluorescence microscopy (Fig. 1C), demonstrated cell-surface as well as likely internalized complexes of DRα1, strongly suggesting binding to DRα1 receptors, which occurs within minutes after in vitro treatment.

DRα1 modulates expression of CD74 and directly inhibits binding of MIF and its downstream effects

To evaluate the relationship between binding of DRα1 and expression of CD74 on the cell surface, human PBMC were incubated with 10 μg DRα1, trypsin-digested DRα1, DR2β1, or DRα1 incubated with FabG4 at a 1:1 molar ratio for 1 h at 37°C and then evaluated by FACS for cell-surface expression of CD74. Results from five HC subjects demonstrated decreased cell-surface expression of CD74 when cells were treated with an intact DRα1 construct. Tryptic digestion destroyed the ability of DRα1 to downregulate cell-surface CD74 expression, whereas DR2β1 had no effect on CD74 cell-surface expression. DRα1-induced downregulation of CD74 cell-surface expression was inhibited by FabG4, suggesting that FabG4 binding to DRα1 blocks the interaction between DRα1 and CD74. Moreover, incubation of PBMC with FabG4 alone significantly increased cell-surface expression of CD74 (Fig. 2A), indicating no interaction between the FabG4 and CD74 or other cell-surface molecules.

Binding and downregulation of CD74 surface expression by DRα1 might have an important regulatory effect on MIF-mediated monocyte activation. In order to determine if DRα1 directly inhibits MIF binding to CD74, we assessed the influence of DRα1 on MIF binding to immunopurified CD74. The immunoprecipitated CD74 complex was incubated for 16 h at 4°C with A488-rhMIF with or without DRα1 or DR2β1. As shown in Fig. 2B, unlabeled DRα1 reduced rhMIF binding to CD74 in a dose-dependent manner, whereas there was negligible inhibition of MIF binding to immunoprecipitated CD74 by 1 nM DR2β1. The PVDF membrane also was probed with anti-CD74 mAb (ln-1) to confirm the presence of CD74 (data not shown).

We sought to determine if this inhibition of binding also suppressed MIF effects on monocytes, such as inhibition of apoptosis after activation (17). As shown in Fig. 2C, human PBMC that were stimulated with LPS and rhMIF and DRα1 for 24 h had significantly higher expression levels of Annexin V on CD11b$^+$ monocytes compared with stimulated cells that were not treated with DRα1, indicating that the DRα1 is blocking the MIF antiapoptosis effect. The frequency of 7-aminoactinomycin D–positive CD11b$^+$ monocytes corresponded with the expression levels of Annexin V staining (Supplemental Fig. 3). These results strongly suggest that HLA-DRα1 has a bifunctional regulatory role in reducing both the accessibility and availability of CD74 for MIF binding, thus reversing its consequent downstream signaling, including resistance to apoptosis as assessed by expression of both Annexin V and 7-aminoactinomycin D.

DRα1 treats clinical EAE by inhibiting monocyte infiltration

We have previously shown enhanced CD74 cell-surface expression on monocytes in mice undergoing EAE (both in the periphery and the CNS) and in subjects with MS, demonstrating that CD74 expression levels are correlated with induction of inflammation (6, 9). To evaluate the ability of DRα1 to treat EAE, which was recently shown to be influenced by MIF, DR*1501-Tg mice were immunized with murine MOG–35–55/CFA/Ptx. Treatment with different concentrations of DRα1 (100, 300, or 500 μg or 1 mg daily × 5) after disease onset at a clinical score of 2 significantly reduced clinical EAE scores in a dose-dependent manner, although treatment with 100 μg appeared to have only a transient effect that lasted for 24 h after the last treatment. In contrast, treatment with DR2β1 did not reverse clinical EAE signs (Fig. 3A). In addition, treatment with trypsin-digested DRα1 did not have a therapeutic effect on the disease (Fig. 3B).

Analysis of spinal cords from DRα1- (1 mg) and vehicle-treated mice 24 h after the last treatment revealed a decreased frequency of CD11b$^+$CD45$^+$cells (infiltrating monocytes and activated microglia) (Fig. 3C). In addition, the expression of cell-surface CD74 on CD11b$^+$CD45$^+$ spinal cord cells was significantly lower in DRα1-treated mice compared with vehicle-treated mice ($p < 0.05$) (Fig. 3D). Taken together, these results demonstrate that the DRα1 not only downregulates CD74 expression, but also inhibits cell migration to the CNS, which contributes to the reversal of clinical signs of EAE.

DRα1–MOG-35–55 acquires secondary structure and has increased potency for treating EAE

In order to increase the therapeutic efficacy of the DRα1 construct, we produced DRα1 constructs bearing a covalently linked N-terminal mMOG-35–55 (DRα1–MOG-35–55) peptide Ag. A comparison of DRα1–MOG-35–55 to DRα1 in vitro revealed that a concentration of 1 μg DRα1–MOG-35–55 was more effective than DRα1 in downregulating CD74 cell-surface expression on human CD11b$^+$ monocytes, with the constructs having equivalent activity at higher concentrations (5 and 10 μg; Fig. 4A).

We reasoned that the difference in downregulation of CD74 could be the result of conformational differences between the two proteins. As a first approach to test this possibility, we evaluated secondary and tertiary structures of these constructs using CD. As shown in Fig. 4B, spectrometric characterization in the near-UV light of the DRα1 construct and the MOG-35–55 peptide using CD revealed a quasi-unfolded, extended conformation with no content of α helix and very low β-sheet secondary structure, given by the absorbances at 193, 208, and 220 nm for α-helix

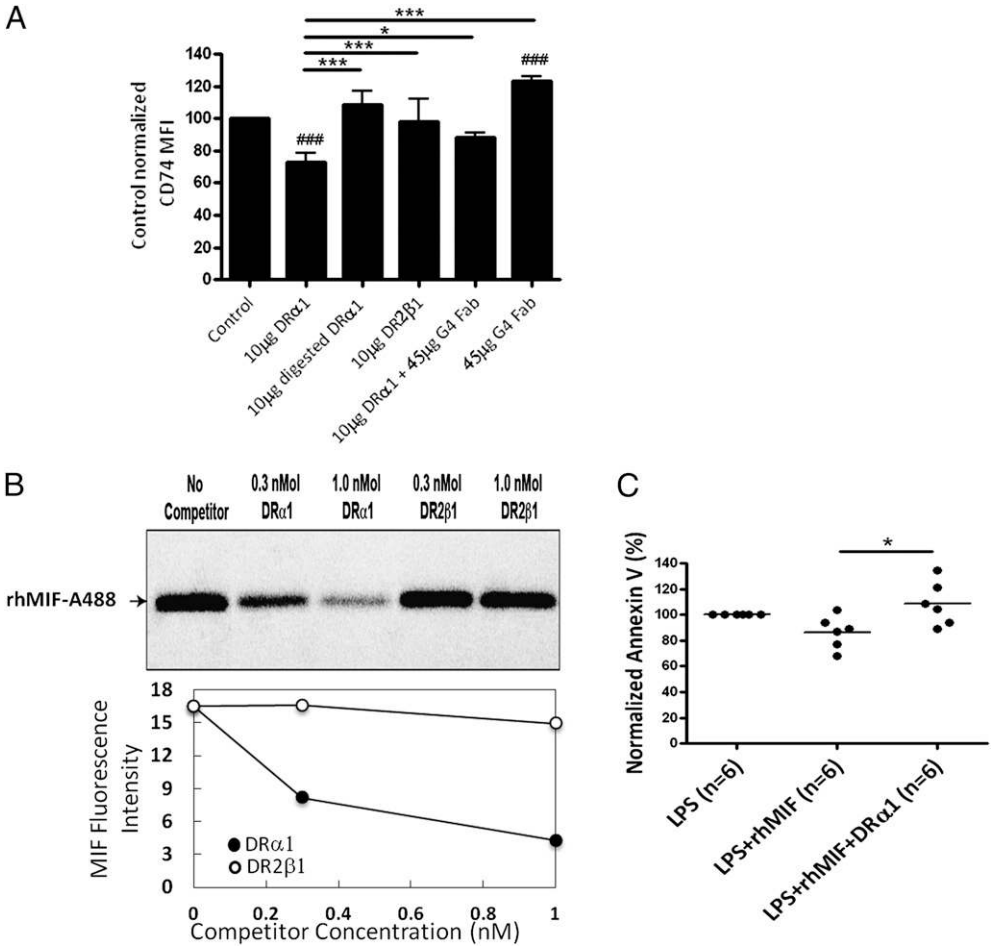

FIGURE 2. DRα1 modulates the cell-surface expression of CD74 and directly inhibits MIF binding. (**A**) PBMC from HC ($n = 5$) were incubated with 10 μg DRα1, 10 μg trypsin-digested DRα1, and 10 μg DR2β1 that was incubated at a 1:1 molar ratio (20 μg) of FabG4 for 2 h at room temperature prior to incubation with cells and 20 μg of FabG4 alone for 1 h at 37˚C. $CD11b^+$ monocytes analyzed for CD74 expression (CD74 mean fluorescence intensity [MFI] was normalized to the untreated sample, 100% of each subject). (**B**) Unlabeled DRα1 (0.3 or 1 nmol), unlabeled DR2β1 (0.3 or 1 nmol), rhMIF-A488 (10 pmol), or a mixture of 10 pmol of rhMIF-A488 and unlabeled constructs were bound for 6 h at 4˚C to immune complexes containing mouse CD74 bound to protein L–adsorbed ln-1 mAb in the presence of 0.01% CHAPS/TEN buffer (pH 7.4). Complexes were then washed extensively with the same buffer and once with TEN buffer only before proteins were eluted with 2% SDS/electrophoresis sample buffer at 95˚C for 7 min. Eluates were separated in 10–20% SDS-PAGE, and the gel was scanned for the chromophore A488 to visualize rhMIF-A488. The binding of rhMIF-A488 to mCD74 was quantified by relative fluorescence intensity. (**C**) Human PBMC from six HC subjects were stimulated with 10 ng/ml LPS with or without 100 ng/ml rhMIF and treated with 10 μg/ml DRα1. The cells were incubated at 37˚C for 24 h and analyzed for Annexin V staining on $CD11b^+$ monocytes. Results were normalized to the LPS-alone treatment of every subject separately. $^*p < 0.05$, $^{***}p < 0.001$, one-way Kruskal-Wallis ANOVA with Dunn multiple comparisons posttest, $^{\#\#\#}p < 0.001$ DRα1 or FabG4 versus control.

and 198 and 218 nm for β-sheets. In contrast, the DRα1–MOG-35–55 construct showed a high content of α helix and β sheet structures similar to that expected for the MHC class II α1 domain from x-ray crystallographic studies (18–23).

Based on these results, we sought to determine whether DRα1–MOG-35–55 had more potency in treating EAE than DRα1. In initial experiments, DR*1501-Tg mice immunized with mMOG-35–55/CFA/Ptx were treated with different concentrations of DRα1–MOG-35–55 (20, 100, or 500 μg daily × 5) after disease onset at a clinical score of 2. All doses of DRα1–MOG-35–55, including 20 μg, significantly reduced clinical EAE scores ($p <$ 0.001) (Supplemental Fig. 4). Evaluation of DRα1 and DRα1–MOG-35–55 treatments demonstrated comparable reduction of EAE scores using 1 mg DRα1 versus 20 μg DRα1–MOG-35–55 (a 50× difference) (Fig. 4C), indicating that the activity of DRα1 was indeed strongly potentiated by the N-terminal MOG-35–55 peptide extension. The DRα1–MOG-35–55 peptide treatment also strongly decreased histological damage of EAE in spinal cord sections (Fig. 4D).

DRα1–MOG-35–55 transiently attenuates MBP-85–99–induced EAE in MBP-TCR/DR2-Tg mice

We previously reported that partial MHC class II constructs containing the MOG-35–55 peptide differed from other constructs in their remarkable ability to treat EAE induced by noncognate encephalitogenic peptides (9). In order to assess if the DRα1 or DRα1–MOG-35–55 constructs might induce this bystander suppression effect, negatively isolated $CD11b^+$ cells were coincubated with CFSE-labeled $CD4^+$ T cells obtained from MBP-85–99 peptide–immunized MBP-TCR/DR2-Tg mice. Isolated $CD11b^+$ cells were cocultured with CFSE-labeled Tg T cells in the presence of free MBP-85–99 peptide, DRα1 or DRα1–MOG-35–55 in 96-well round-bottom plates for 3 d. As expected, $CD11b^+$ cells induced proliferation of CFSE-labeled T cells (22% positive) in the presence of added MBP-85–99 peptide (Fig. 5A). However, incubation of $CD11b^+$ APC plus $CD4^+$ T cells with DRα1–MOG-35–55 did not induce a significant proliferation response greater than medium alone. Of critical

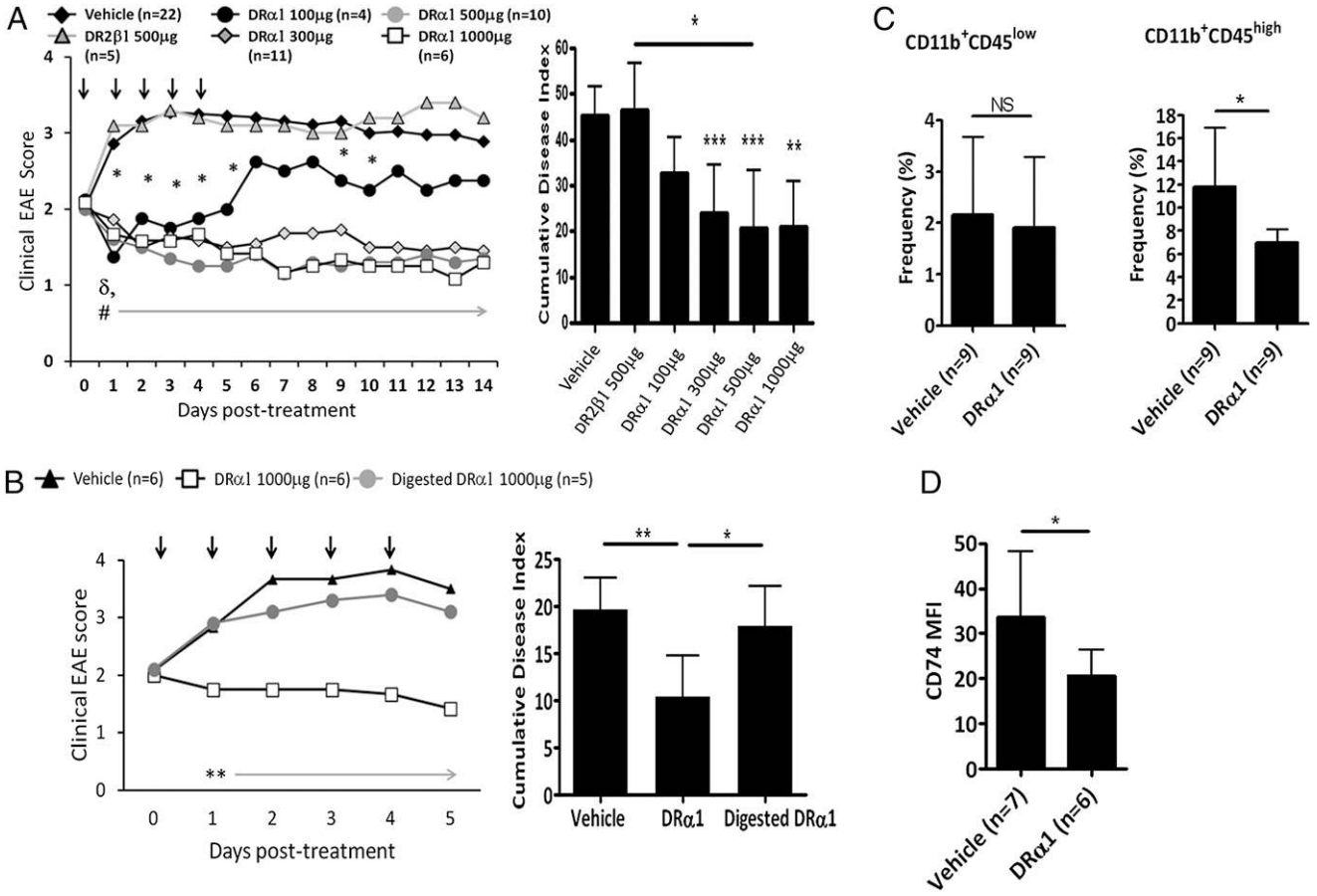

FIGURE 3. DRα1 treats clinical EAE. (**A**) DR*1501-Tg mice with mMOG-35–55–induced EAE were treated after disease onset at a clinical score of 2 with vehicle, DR2β1 (500 μg), or DRα1 (100, 300, and 500 μg and 1 mg daily × 5; arrows). Mean clinical EAE daily disease (*left panel*) and CDI scores (*right panel*) are shown. (**B**) DR*1501-Tg mice with mMOG-35–55–induced EAE were treated after disease onset at a clinical score of 2 with vehicle, DRα1, or trypsin-digested DRα1 (1 mg daily × 5). Mean clinical EAE daily disease (*left panel*) and CDI scores (*right panel*) are shown. $^{*}p < 0.05$ (DR-α1 100 μg versus vehicle), $^{\#}p < 0.0003$, $^{\delta}p < 0.04$ (DR-α1 300–1000 μg versus vehicle and DR2-β1, respectively); $^{*}p < 0.05$, $^{**}p < 0.01$, $^{***}p < 0.001$. Daily mean scores were analyzed by Mann–Whitney *U* and mean CDI by one-way ANOVA with Tukey posttest and nonparametric one-way Kruskal Wallis ANOVA with Dunn multiple comparisons posttest. (**C**) Frequency of $CD11b^{+}CD45^{+}$ cells in spinal cord was analyzed 24 h after last vehicle or DRα1-treated DR*1501-Tg mice. (**D**) Frequency of cell-surface CD74 on $CD11b^{+}CD45^{+}$ cells in spinal cord was analyzed 24 h after last vehicle- or DRα1-treated DR*1501-Tg mice. $^{*}p < 0.05$, Student *t* test (C, D). MFI, mean fluorescence intensity.

importance, a significantly reduced proliferation response of activated T cells was observed when free MBP-85–99 peptide was added to the DRα1 or DRα1–MOG-35–55–armed $CD11b^{+}$ cells (~7% positive, Fig. 5A), clearly demonstrating a substantial degree of bystander suppression.

In order to confirm this bystander effect in vivo, EAE was induced with MBP-85–99/CFA/Ptx in MBP-TCR/DR2-Tg mice. Treatment with DRα1–MOG-35–55 (100 μg, daily × 5) after disease onset at a clinical score of 2 significantly reduced clinical EAE scores compared with vehicle-treated mice on days 1–4 posttreatment ($p < 0.05$) (Fig. 5B). Thus, DRα1–MOG-35–55 treatment transiently attenuated the MBP-induced disease in the MBP-TCR/DR2-Tg mice. Although the treatment effect did not appear to be as potent as in the DR*1501-Tg mice with MOG-35–55–induced EAE, these data demonstrate that DRα1–MOG-35–55 has a significant bystander effect on MBP–TCR-Tg T cells and on MBP-95–99–induced EAE.

Discussion

The MHC encodes highly polymorphic proteins that bind peptides for presentation to $CD4^{+}$ and $CD8^{+}$ TCRs (24, 25). However, several of the MHC proteins are not polymorphic, including Ii (CD74) and the DRα-chain. We demonstrate a heretofore unrecognized immunoregulatory interaction between these two highly conserved MHC proteins in which DRα1 constructs, upon binding to CD74, inhibit MIF binding and signaling and treat ongoing clinical and histological signs of EAE. We further report that the therapeutic potency of the DRα1 construct could be enhanced by addition of a peptide extension at the N terminus.

Although the function of the CD74 invariant chain as an MHC class II chaperone has been studied extensively (14, 26), the role of the cell-surface form of CD74 in the immune response is not fully understood. It was shown previously that CD74 forms a functional signal transduction complex with CD44, CXCR2, and CXCR4 to transduce MIF signaling (3–5, 27). Recently, we reported that CD74 surface expression on $CD11b^{+}$ monocytes is upregulated in mice with EAE and subjects with MS (6). However, very little is known about the interaction of CD74 and MHC class II on the surface of APC during the steady state or inflammation. Consistent with the prior literature that studied intracellular interactions among CD74, HLA-DM, and DRα during peptide loading of nascent MHC class II molecules (15–17, 28–30), we recently demonstrated that DRα1 constructs could bind to immunoprecipitated CD74 (9). Hence, we used this construct to study cell-surface interactions of DRα1 with CD74 and its possible effects on MIF binding and signaling. In this study, we report that the

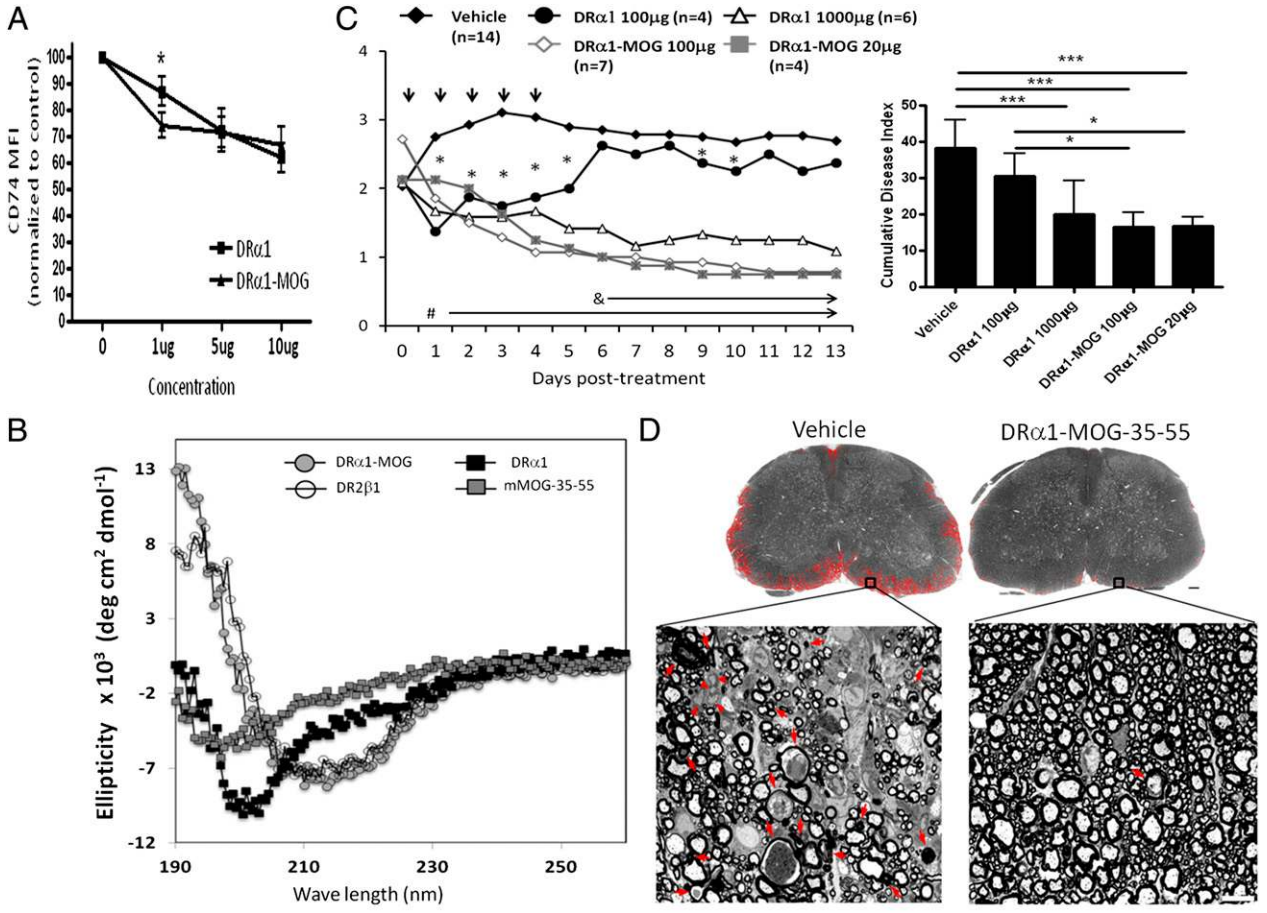

FIGURE 4. DRα1–MOG-35–55 has increased potency for treating EAE. (**A**) PBMC from HC ($n = 3$) were incubated with DRα1 or DRα1–MOG-35–55 at different concentrations (1, 5, and 10 μg) and $CD11b^+$ monocytes analyzed for CD74 expression (CD74 mean fluorescence intensity [MFI] were normalized to the untreated sample, 100% of each subject). $^*p < 0.05$, Student t test. (**B**) Far-UV spectra of DRα1, DRα1–MOG-35–55, and DR2β1 constructs and mouse MOG-35–55 peptide in 20 mM Tris (pH 8.5) at a concentration of 1 mg/ml. Spectra were measured on an AVIV spectropolarimeter at 0.5-nm bandwidth using a 0.1-cm light path. Blank CD spectra (20 mM Tris [pH 8.5]) were determined and subtracted from the sample spectra. (**C**) DR*1501 mice with EAE were treated after disease onset at a clinical score of 2 with vehicle (five daily treatments), DRα1 (100 μg × 5), DRα1 (1000 μg × 5), DRα1–MOG-35–55 (100 μg × 5), and DRα1–MOG-35–55 (20 μg × 5). *Left panel*: daily mean clinical EAE disease scores. $^*p < 0.05$, DRα1 (100 μg) versus vehicle), $^{\&}p < 0.03$, DRα1–MOG-35–55 (100 μg) and DRα1–MOG-35–55 (20 μg) versus DRα1 (100 μg), $^{\#}p < 0.001$ DRα1 (1000 μg), DRα1–MOG-35–55 (100 μg), and DRα1–MOG-35–55 (20 μg) versus vehicle. *Right panel*: statistical comparisons of CDIs. $^*p < 0.05$, $^{***}p < 0.0001$. Daily mean scores were analyzed by Mann–Whitney U and mean CDI by one-way ANOVA with Tukey posttest. (**D**) Spinal cord sections from EAE DR*1501-Tg mice, as visualized after toluidine blue staining, either from vehicle- or DRα1–MOG-35–55–treated mice. The areas of tissue damage in white matter are in red. Scale bar, 100 μm. High-power view of small areas of lumbar spinal cord (black rectangles) show axons that are undergoing demyelination (red arrow) and cellular infiltration (red arrowhead). Scale bar, 10 μm.

DRα1 construct can bind to both immunoprecipitated CD74 and H2-M. The fact that the trypsin-digested DRα1 could bind only to H2-M but not to CD74 suggests that the binding of DRα1 to CD74 is either conformationally dependent or that the trypsin digestion destroyed the binding site to CD74. Future experiments will determine if overlapping peptides of the DRα1 domain can bind to CD74. Conformation-dependent binding of DRα1 to CD74 might indicate that binding sites on DRα1 for CD74 and H2-M are distinct. Because H2-M is not expressed on the cell surface and thus would not be available for binding, we focused on the interaction of CD74 with the DRα1 domain. The DRα1 construct not only could bind human and mouse $CD11b^+$ monocytes, but also could downregulate surface expression of CD74. Interestingly, although DRα1 bound better to human versus mouse monocytes, there was less efficient downregulation of CD74 levels on human monocytes, possibly due to a faster recycling of the cell-surface CD74 (31). This binding could be inhibited with a specific Fab to DRα1 that apparently could block the binding site on DRα1 for CD74. We further show that this binding of DRα1 to immunoprecipitated CD74 could inhibit binding of MIF to CD74 and its downstream signaling effects.

It was previously demonstrated that during the assembly of MHC class II in the endoplasmic reticulum, the homotrimeric CD74 invariant chain initially binds single MHC class II α-chains and that this complex serves as a scaffold for subsequent binding of the β-chains (29). We demonstrate in this study that the immunoprecipitated cell-surface homotrimeric CD74 complex reiterates the initial binding to the DRα1 construct but does not bind to the DR2β1 construct (9). We would thus speculate that the binding of the DRα1 construct to CD74 and subsequent blocking of MIF binding and signaling might represent a natural immunoregulatory role for the DRα-chain in terminating MIF-dependent inflammation. This novel concept is supported by the binding of the *Staphylococcal* toxic shock syndrome toxin 1 (TSST-1) to the DRα-chain, in which the TSST-1 binding site on HLA-DRα1 partially overlaps with the DRα1/CD74 binding site (32). These data, coupled with the report by Calandra et al. (33) showing that MIF is a mediator of the activation of immune cells by TSST-1, suggests

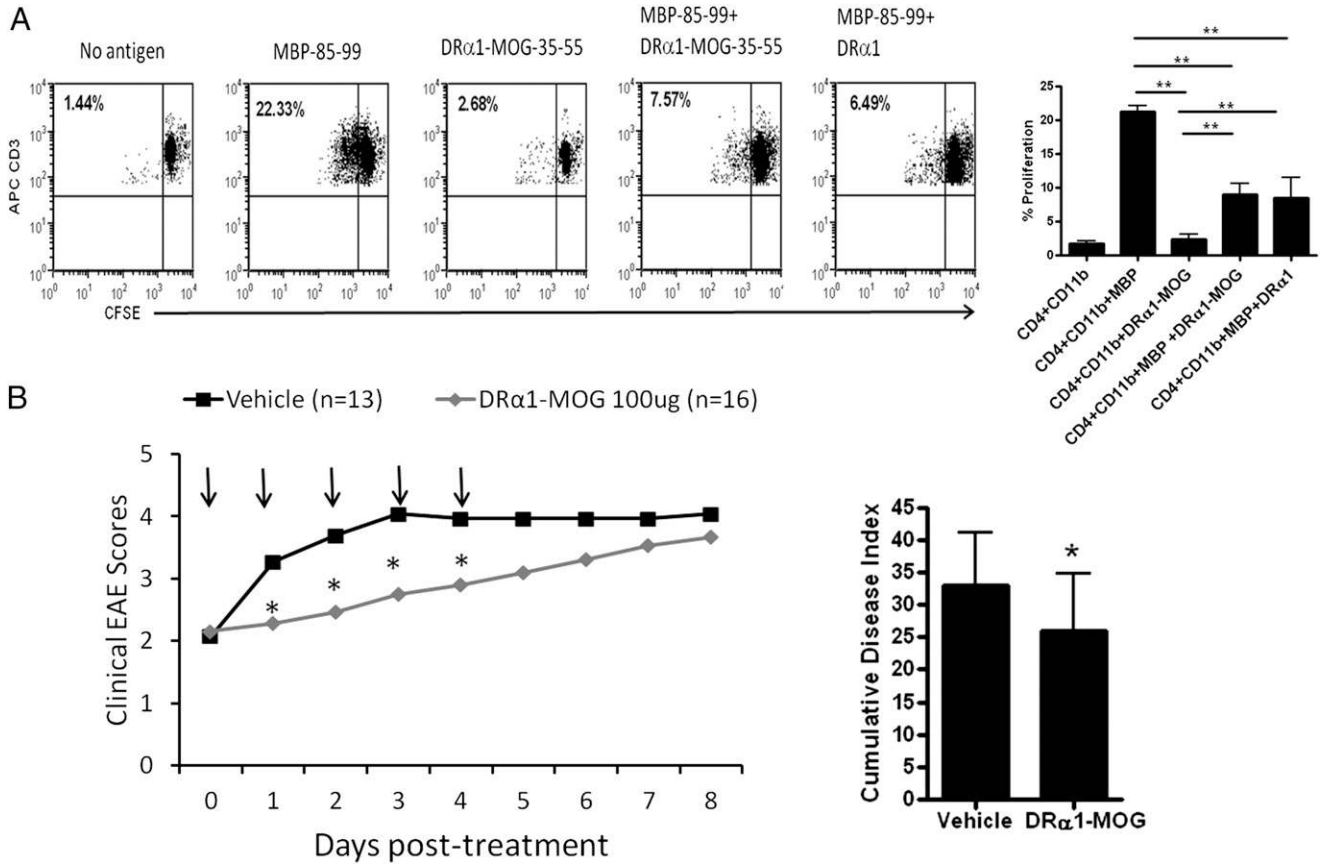

FIGURE 5. DRα1–MOG-35–55 inhibits MBP-85–99 peptide–induced proliferation of activated T cells and transiently attenuates MBP-85–99–induced EAE in MBP-TCR/DR2-Tg mice. (**A**) $CD4^+$ and $CD11b^+$ cells were isolated from the spleens of MBP-85–99/CFA-immunized MBP-TCR/DR2 mice. Sorted $CD11b^+$ cells were cultured with CSFE-labeled primed T cells from the same mice at a 1:2 ratio ($CD4^+/CD11b^+$) in the presence or absence of free MBP-85–99 peptide, DRα1–MOG-35–55, or a combination of MBP-85–99 peptide and DRα1-MOG-35–55 or DRα1. After 3 d of culture, cells were washed and evaluated by FACSCalibur (BD Biosciences) for CD3 expression and CFSE dilution. (**B**) MBP-TCR/DR2-Tg mice with MBP-85–99–induced EAE were treated after disease onset at a clinical score of 2 with vehicle or DRα1–MOG-35–55 (500 μg daily × 5, black arrows). Mean clinical EAE daily disease scores (*left panel*) and CDI (*right panel*) are shown. $*p < 0.05$.

the possibility that TSST-1 is blocking the binding of HLA-DRα to CD74, which in turn makes more CD74 available to bind MIF, thus inducing the toxic shock.

We further demonstrate that the DRα1 construct could be used as a therapeutic reagent in a CNS disease model that was shown to be mediated by MIF (34–36). Treatment with DRα1 reduced the frequency of activated microglia and infiltrating macrophages in the spinal cord and reduced the CD74 level of expression on these cells compared with those from vehicle-treated mice. We also showed a correlation between the ability of different constructs to bind to and downregulate CD74 expression on $CD11b^+$ cells in vitro and their ability to treat EAE. Only the DRα1 construct, but not its peptide digest or the DR2β1 construct, could bind to and downregulate CD74 expression and treat EAE. Our data demonstrate that DRα1 constructs have a bifunctional role, downregulating CD74 surface expression and inhibiting MIF binding to CD74. These two functions might have distinct effects on the cell. DRα1 treatment reduces but does not completely downregulate CD74 surface expression (only ~30%), providing a detectable phenotypic change. However, this partially reduced availability of CD74 alone would not seem sufficient to account for observed inhibition of MIF effects. Alternatively, we would speculate that competitive DRα1 inhibition of MIF binding to remaining cell-surface CD74 might be the more potent mechanism for therapeutic effects of DRα1 on EAE. Relevant to this issue, only a fraction (~5%) of surface CD74 on monocytes exists free of MHC class II (37), and it is conceivable that the remaining 95% of class II–associated CD74 would not be amenable to MIF binding due to occupancy by natural DRα present in cell-surface MHC class II. If true, only the remaining class II–unassociated CD74 would mediate MIF effects, thus reducing the scope of regulatory interactions needed for effective DRα1 treatment.

In order to enhance the potency of the DRα1 construct and potentially engage neuroantigen peptide–dependent effects, we covalently linked a peptide extension of MOG-35–55 to the N terminus of DRα1. We have previously reported that partial MHC class II β1α1 constructs containing the MOG-35–55 peptide linked to the N terminus of DR2β1α1 are more potent therapeutic reagents than other peptide extensions or empty constructs (9). Our current report clearly demonstrates that a relative low dose of 1 μg of the DRα1–MOG-35–55 construct in vitro is more potent in downregulating CD74 surface expression than the same concentration of the DRα1 construct.

The secondary structures of DRα1, DRα1–MOG-35–55, DR2β1, and free MOG-35–55 peptide were explored by CD (Fig. 4B). Crystal structures determined for MHC class II proteins show that they are organized into two well defined regions, each adopting specific folded structures. The α1 and β1 domains, which contain α-helices sitting atop a β-pleated sheet structure, contribute to the peptide Ag binding groove and are located distal to the membrane, whereas the α2 and β2 domain are Ig-like structures positioned proximal to the cell membrane (18–23). We here present

new data indicating that DRα1 in the absence of covalently tethered peptide Ag lacks the well-defined secondary structure characteristic of the α1 domain within MHC class II, whereas the DR2β1 domain retains much of the secondary structure of the β1-domain within the MHC class II molecule. When linked to the N terminus of the DRα1 protein, the MOG peptide induced changes in secondary structure, including increased α-helix and β-sheet content that is not present in the DRα1 or the MOG-35–55 peptide alone. To this point, other studies have shown that the MOG peptide displays an extended conformation in solution with a not fully formed α-helix at the N terminus (38). To the best of our knowledge, our CD spectroscopy study is the first demonstration of a peptide-triggered conformational change observed in an isolated MHC class II domain.

Taken in the context of an empty MHC class II molecule, these results might suggest that the α1 is present as an extended entity and that the β1 might exist as a partially folded structural domain. If this is actually the case, it might also explain why it has been difficult in practice to crystallize empty MHC class II molecules (because its success depends on properly folded polypeptides) unless they are provided with an antigenic peptide bound to the Ag-binding groove. There is ample evidence suggesting that upon peptide binding, class II molecules undergo dramatic conformational changes induced by the peptide (20, 39–43). Other studies have relied on molecular probes such as mAbs and toxins that bind specifically to MHC class II to explore structural changes in the involved MHC class II molecules (44, 45). The region that undergoes the most striking changes in conformation is the α1 domain and to a lesser extent, the β1 domain. By a combination of molecular dynamics simulation and biochemical experimentation, Painter et al. (41) showed that when the peptide is removed, substantial changes in structure occur in the α1 domain between residues 15 and 90, but only local changes occur in the β1 domain, mostly within residues 50–70 at the center of the α-helix. The results described in these studies are confirmed by our CD spectroscopic data showing a loss of overall structure within the α1 domain and loss of α-helix conformation with a high content of anti-parallel β-sheet region in the β1 domain.

Many cellular proteins are intrinsically disordered and undergo folding, complete or partial, upon binding to their physiological partners, and a great majority of these disordered proteins play a relevant role in signaling cascades, acting as hubs of protein interaction networks enabling them to interact promiscuously with a wide variety of targets (46–48). How the MOG-35–55 peptide triggers this global conformational change in the DRα1 domain is the subject of our ongoing research.

Treatment of clinical EAE with the DRα1–MOG-35–55 construct also revealed at least a 50× increase in potency compared with the DRα1 construct (Fig. 4C, 20 versus 1000 μg, respectively). In a concurrent study, we recently demonstrated that the DRα1-MOG-35–55 construct could treat experimental stroke. Four daily treatments with DRα1-MOG-35–55 reduced infarct size by 40% in the cortex, striatum, and hemisphere, inhibited the migration of activated $CD11b^{+}CD45^{high}$ cells from the periphery to the brain, and reversed splenic atrophy (49). Hence, this novel construct could treat different CNS diseases that involve migration of immune cells from the periphery to both the brain (stroke) and spinal cord (EAE). In addition, we report in this study that the DRα1 and DRα1–MOG-35–55 constructs could inhibit MBP-85–99 peptide–induced proliferation of activated T cells when cocultured with primed $CD11b^{+}$ cells as well as transiently attenuate MBP-85–99–induced EAE for several days in MBP-TCR/DR2-Tg mice. We have shown recently that the RTL1000 construct containing the MOG-35–55 peptide could treat EAE in this same model, probably through a similar bystander tolerance mechanism (9). The lack of complete treatment of the DRα1–MOG-35–55 construct compared with the RTL constructs might be attributed to the difference in the disease severity between the two experiments (average peak of disease for the vehicle-treated mice in the RTL experiment was 3.5 ± 0.5 versus 4.4 ± 0.6 in the current experiment).

In summary, we demonstrate that the DRα1 domain could treat EAE by inhibiting MIF binding to CD74 on monocytes, thus blocking its proinflammatory effects. Because the DRα1 amino acid sequence is conserved in humans, the recombinant DRα1–MOG-35–55 construct potentially represents an immunotherapy that would not require HLA screening prior to use. Potency of the DRα1 domain could be destroyed by trypsin digestion and could be enhanced by addition of a peptide extension (MOG-35–55 peptide) that we hypothesize induced α-helix and β-strand structures not present in DRα1 alone. In addition, this novel therapeutic DRα1–MOG-35–55 construct could represent a new approach for regulating MIF and the immune response in CNS and other inflammatory conditions.

Acknowledgments

We thank Melissa S. Barber for assistance with manuscript submission.

Disclosures

The authors have no financial conflicts of interest.

References

1. Leng, L., C. N. Metz, Y. Fang, J. Xu, S. Donnelly, J. Baugh, T. Delohery, Y. Chen, R. A. Mitchell, and R. Bucala. 2003. MIF signal transduction initiated by binding to CD74. *J. Exp. Med.* 197: 1467–1476.
2. Cresswell, P. 1996. Invariant chain structure and MHC class II function. *Cell* 84: 505–507.
3. Bernhagen, J., R. Krohn, H. Lue, J. L. Gregory, A. Zernecke, R. R. Koenen, M. Dewor, I. Georgiev, A. Schober, L. Leng, et al. 2007. MIF is a noncognate ligand of CXC chemokine receptors in inflammatory and atherogenic cell recruitment. *Nat. Med.* 13: 587–596.
4. Schwartz, V., H. Lue, S. Kraemer, J. Korbiel, R. Krohn, K. Ohl, R. Bucala, C. Weber, and J. Bernhagen. 2009. A functional heteromeric MIF receptor formed by CD74 and CXCR4. *FEBS Lett.* 583: 2749–2757.
5. Shi, X., L. Leng, T. Wang, W. Wang, X. Du, J. Li, C. McDonald, Z. Chen, J. W. Murphy, E. Lolis, et al. 2006. CD44 is the signaling component of the macrophage migration inhibitory factor-CD74 receptor complex. *Immunity* 25: 595–606.
6. Benedek, G., R. Meza-Romero, S. Andrew, L. Leng, G. G. Burrows, D. Bourdette, H. Offner, R. Bucala, and A. A. Vandenbark. 2013. Partial MHC class II constructs inhibit MIF/CD74 binding and downstream effects. *Eur. J. Immunol.* 43: 1309–1321.
7. Metodieva, G., N. C. Nogueira-de-Souza, C. Greenwood, K. Al-Janabi, L. Leng, R. Bucala, and M. V. Metodiev. 2013. CD74-dependent deregulation of the tumor suppressor scribble in human epithelial and breast cancer cells. *Neoplasia* 15: 660–668.
8. Stein, R., M. J. Mattes, T. M. Cardillo, H. J. Hansen, C. H. Chang, J. Burton, S. Govindan, and D. M. Goldenberg. 2007. CD74: a new candidate target for the immunotherapy of B-cell neoplasms. *Clin. Cancer Res.* 13: 5556s–5563s.
9. Vandenbark, A. A., R. Meza-Romero, G. Benedek, S. Andrew, J. Huan, Y. K. Chou, A. C. Buenafe, R. Dahan, Y. Reiter, J. L. Mooney, et al. 2013. A novel regulatory pathway for autoimmune disease: binding of partial MHC class II constructs to monocytes reduces CD74 expression and induces both specific and bystander T-cell tolerance. *J. Autoimmun.* 40: 96–110.
10. Vandenbark, A. A., C. Rich, J. Mooney, A. Zamora, C. Wang, J. Huan, L. Fugger, H. Offner, R. Jones, and G. G. Burrows. 2003. Recombinant TCR ligand induces tolerance to myelin oligodendrocyte glycoprotein 35-55 peptide and reverses clinical and histological signs of chronic experimental autoimmune encephalomyelitis in HLA-DR2 transgenic mice. *J. Immunol.* 171: 127–133.
11. Bebo, B. F., Jr., A. A. Vandenbark, and H. Offner. 1996. Male SJL mice do not relapse after induction of EAE with PLP 139-151. *J. Neurosci. Res.* 45: 680–689.
12. Bernhagen, J., R. A. Mitchell, T. Calandra, W. Voelter, A. Cerami, and R. Bucala. 1994. Purification, bioactivity, and secondary structure analysis of mouse and human macrophage migration inhibitory factor (MIF). *Biochemistry* 33: 14144–14155.
13. Sinha, S., L. Miller, S. Subramanian, O. J. McCarty, T. Proctor, R. Meza-Romero, J. Huan, G. G. Burrows, A. A. Vandenbark, and H. Offner. 2010. Binding of recombinant T cell receptor ligands (RTL) to antigen presenting cells prevents upregulation of CD11b and inhibits T cell activation and transfer of experimental autoimmune encephalomyelitis. *J. Neuroimmunol.* 225: 52–61.

14. Cresswell, P. 1994. Assembly, transport, and function of MHC class II molecules. *Annu. Rev. Immunol.* 12: 259–293.
15. Fling, S. P., B. Arp, and D. Pious. 1994. HLA-DMA and -DMB genes are both required for MHC class II/peptide complex formation in antigen-presenting cells. *Nature* 368: 554–558.
16. Morris, P., J. Shaman, M. Attaya, M. Amaya, S. Goodman, C. Bergman, J. J. Monaco, and E. Mellins. 1994. An essential role for HLA-DM in antigen presentation by class II major histocompatibility molecules. *Nature* 368: 551–554.
17. Mitchell, R. A., H. Liao, J. Chesney, G. Fingerle-Rowson, J. Baugh, J. David, and R. Bucala. 2002. Macrophage migration inhibitory factor (MIF) sustains macrophage proinflammatory function by inhibiting p53: regulatory role in the innate immune response. *Proc. Natl. Acad. Sci. USA* 99: 345–350.
18. Günther, S., A. Schlundt, J. Sticht, Y. Roske, U. Heinemann, K. H. Wiesmüller, G. Jung, K. Falk, O. Rötzschke, and C. Freund. 2010. Bidirectional binding of invariant chain peptides to an MHC class II molecule. *Proc. Natl. Acad. Sci. USA* 107: 22219–22224.
19. Kim, C. Y., H. Quarsten, E. Bergseng, C. Khosla, and L. M. Sollid. 2004. Structural basis for HLA-DQ2-mediated presentation of gluten epitopes in celiac disease. *Proc. Natl. Acad. Sci. USA* 101: 4175–4179.
20. Murthy, V. L., and L. J. Stern. 1997. The class II MHC protein HLA-DR1 in complex with an endogenous peptide: implications for the structural basis of the specificity of peptide binding. *Structure* 5: 1385–1396.
21. Painter, C. A., M. P. Negroni, K. A. Kellersberger, Z. Zavala-Ruiz, J. E. Evans, and L. J. Stern. 2011. Conformational lability in the class II MHC 310 helix and adjacent extended strand dictate HLA-DM susceptibility and peptide exchange. *Proc. Natl. Acad. Sci. USA* 108: 19329–19334.
22. Scott, C. A., P. A. Peterson, L. Teyton, and I. A. Wilson. 1998. Crystal structures of two I-Ad-peptide complexes reveal that high affinity can be achieved without large anchor residues. *Immunity* 8: 319–329.
23. Stern, L. J., J. H. Brown, T. S. Jardetzky, J. C. Gorga, R. G. Urban, J. L. Strominger, and D. C. Wiley. 1994. Crystal structure of the human class II MHC protein HLA-DR1 complexed with an influenza virus peptide. *Nature* 368: 215–221.
24. Klein, J., and A. Sato. 2000. The HLA system. Second of two parts. [Published erratum appears in 2000 *N. Engl. J. Med.* 343: 1504.] *N. Engl. J. Med.* 343: 782–786.
25. Klein, J., and A. Sato. 2000. The HLA system. First of two parts. *N. Engl. J. Med.* 343: 702–709.
26. Sant, A. J., and J. Miller. 1994. MHC class II antigen processing: biology of invariant chain. *Curr. Opin. Immunol.* 6: 57–63.
27. Calandra, T., and T. Roger. 2003. Macrophage migration inhibitory factor: a regulator of innate immunity. *Nat. Rev. Immunol.* 3: 791–800.
28. Koch, N., M. Zacharias, A. König, S. Temme, J. Neumann, and S. Springer. 2011. Stoichiometry of HLA class II-invariant chain oligomers. *PLoS ONE* 6: e17257.
29. Neumann, J., and N. Koch. 2005. Assembly of major histocompatibility complex class II subunits with invariant chain. *FEBS Lett.* 579: 6055–6059.
30. Pos, W., D. K. Sethi, M. J. Call, M. S. Schulze, A. K. Anders, J. Pyrdol, and K. W. Wucherpfennig. 2012. Crystal structure of the HLA-DM-HLA-DR1 complex defines mechanisms for rapid peptide selection. *Cell* 151: 1557–1568.
31. Moldenhauer, G., C. Henne, J. Karhausen, and P. Möller. 1999. Surface-expressed invariant chain (CD74) is required for internalization of human leucocyte antigen-DR molecules to early endosomal compartments. *Immunology* 96: 473–484.
32. Jasanoff, A., G. Wagner, and D. C. Wiley. 1998. Structure of a trimeric domain of the MHC class II-associated chaperonin and targeting protein Ii. *EMBO J.* 17: 6812–6818.
33. Calandra, T., L. A. Spiegel, C. N. Metz, and R. Bucala. 1998. Macrophage migration inhibitory factor is a critical mediator of the activation of immune cells by exotoxins of Gram-positive bacteria. *Proc. Natl. Acad. Sci. USA* 95: 11383–11388.
34. Cox, G. M., A. P. Kithcart, D. Pitt, Z. Guan, J. Alexander, J. L. Williams, T. Shawler, N. M. Dagia, P. G. Popovich, A. R. Satoskar, and C. C. Whitacre. 2013. Macrophage migration inhibitory factor potentiates autoimmune-mediated neuroinflammation. *J. Immunol.* 191: 1043–1054.
35. Denkinger, C. M., M. Denkinger, J. J. Kort, C. Metz, and T. G. Forsthuber. 2003. In vivo blockade of macrophage migration inhibitory factor ameliorates acute experimental autoimmune encephalomyelitis by impairing the homing of encephalitogenic T cells to the central nervous system. *J. Immunol.* 170: 1274–1282.
36. Powell, N. D., T. L. Papenfuss, M. A. McClain, I. E. Gienapp, T. M. Shawler, A. R. Satoskar, and C. C. Whitacre. 2005. Cutting edge: macrophage migration inhibitory factor is necessary for progression of experimental autoimmune encephalomyelitis. *J. Immunol.* 175: 5611–5614.
37. Wraight, C. J., P. van Endert, P. Möller, J. Lipp, N. R. Ling, I. C. MacLennan, N. Koch, and G. Moldenhauer. 1990. Human major histocompatibility complex class II invariant chain is expressed on the cell surface. *J. Biol. Chem.* 265: 5787–5792.
38. Albouz-Abo, S., J. C. Wilson, C. C. Bernard, and M. von Itzstein. 1997. A conformational study of the human and rat encephalitogenic myelin oligodendrocyte glycoprotein peptides 35-55. *Eur. J. Biochem.* 246: 59–70.
39. Chervonsky, A. V., R. M. Medzhitov, L. K. Denzin, A. K. Barlow, A. Y. Rudensky, and C. A. Janeway, Jr. 1998. Subtle conformational changes induced in major histocompatibility complex class II molecules by binding peptides. *Proc. Natl. Acad. Sci. USA* 95: 10094–10099.
40. Neveu, R., C. Auriault, G. Angyalosi, and B. Georges. 2002. Evidences of conformational changes in class II Major Histocompatibility Complex molecules that affect the immunogenicity. *Mol. Immunol.* 38: 661–667.
41. Painter, C. A., A. Cruz, G. E. López, L. J. Stern, and Z. Zavala-Ruiz. 2008. Model for the peptide-free conformation of class II MHC proteins. *PLoS ONE* 3: e2403.
42. Sato, A. K., J. A. Zarutskie, M. M. Rushe, A. Lomakin, S. K. Natarajan, S. Sadegh-Nasseri, G. B. Benedek, and L. J. Stern. 2000. Determinants of the peptide-induced conformational change in the human class II major histocompatibility complex protein HLA-DR1. *J. Biol. Chem.* 275: 2165–2173.
43. Zarutskie, J. A., A. K. Sato, M. M. Rushe, I. C. Chan, A. Lomakin, G. B. Benedek, and L. J. Stern. 1999. A conformational change in the human major histocompatibility complex protein HLA-DR1 induced by peptide binding. *Biochemistry* 38: 5878–5887.
44. Carven, G. J., S. Chitta, I. Hilgert, M. M. Rushe, R. F. Baggio, M. Palmer, J. E. Arenas, J. L. Strominger, V. Horejsi, L. Santambrogio, and L. J. Stern. 2004. Monoclonal antibodies specific for the empty conformation of HLA-DR1 reveal aspects of the conformational change associated with peptide binding. *J. Biol. Chem.* 279: 16561–16570.
45. McCormick, J. K., T. J. Tripp, A. S. Llera, E. J. Sundberg, M. M. Dinges, R. A. Mariuzza, and P. M. Schlievert. 2003. Functional analysis of the TCR binding domain of toxic shock syndrome toxin-1 predicts further diversity in MHC class II/superantigen/TCR ternary complexes. *J. Immunol.* 171: 1385–1392.
46. Cumberworth, A., G. Lamour, M. M. Babu, and J. Gsponer. 2013. Promiscuity as a functional trait: intrinsically disordered regions as central players of interactomes. *Biochem. J.* 454: 361–369.
47. Dunker, A. K., M. S. Cortese, P. Romero, L. M. Iakoucheva, and V. N. Uversky. 2005. Flexible nets. The roles of intrinsic disorder in protein interaction networks. *FEBS J.* 272: 5129–5148.
48. Wright, P. E., and H. J. Dyson. 2009. Linking folding and binding. *Curr. Opin. Struct. Biol.* 19: 31–38.
49. Benedek, G., W. Zhu, N. Libal, A. Casper, X. Yu, R. Meza-Romero, A. A. Vandenbark, N. J. Alkayed, and H. Offner. 2014. A novel HLA-DRα1-MOG-35-55 construct treats experimental stroke. *Metab. Brain Dis.* 29: 37–45.